nature cell biology

LETTER

N^6-methyladenosine modification destabilizes developmental regulators in embryonic stem cells

Yang Wang[1], Yue Li[2], Julia I. Toth[1], Matthew D. Petroski[1], Zhaolei Zhang[2,3] and Jing Crystal Zhao[1,4]

N^6-methyladenosine (m^6A) has been identified as the most abundant internal modification of messenger RNA in eukaryotes[1]. m^6A modification is involved in cell fate determination in yeast[2,3] and embryo development in plants[4,5]. Its mammalian function remains unknown but thousands of mammalian mRNAs and long non-coding RNAs (lncRNAs) show m^6A modification[6,7] and m^6A demethylases are required for mammalian energy homeostasis and fertility[8,9]. We identify two proteins, the putative m^6A MTase, methyltransferase-like 3 (Mettl3; ref. 10), and a related but uncharacterized protein Mettl14, that function synergistically to control m^6A formation in mammalian cells. Knockdown of *Mettl3* and *Mettl14* in mouse embryonic stem cells (mESCs) led to similar phenotypes, characterized by lack of m^6A RNA methylation and lost self-renewal capability. A large number of transcripts, including many encoding developmental regulators, exhibit m^6A methylation inversely correlated with mRNA stability and gene expression. The human antigen R (HuR) and microRNA pathways were linked to these effects. This gene regulatory mechanism operating in mESCs through m^6A methylation is required to keep mESCs at their ground state and may be relevant to thousands of mRNAs and lncRNAs in various cell types.

RNA and DNA MTases share structural motifs required to transfer methyl groups from *S*-adenosyl-L-methionine (SAM) to nucleic acid. Previously, two mammalian m^6A MTases, *Mettl3* and *Mettl14*, were predicted computationally on the basis of conservation of the SAM-binding domain and phylogenetic analysis[11,12]. Mettl3 purified from HeLa cell nuclear extracts functions as a putative MTase (ref. 10). Mettl14 remains uncharacterized. A recent study reported altered RNA splicing in Mettl3 knockdown (KD) HeLa cells[7], but as yet no direct evidence links Mettl3 to m^6A formation.

An NCBI Blast Protein sequence analysis revealed greater than 35% sequence homology of the MTase domain between Mettl3 and Mettl14 (Fig. 1a), suggesting that both are MTases. To investigate this possibility we constructed short hairpin RNAs (shRNAs) targeting *Mettl3* or *Mettl14* and generated mESC lines harbouring efficient KD of each (Fig. 1b). We then used two independent methods to determine m^6A levels in KD mESCs. First, immunoblotting of RNA samples using a highly specific α-m^6A antibody[6,7] indicated decreased m^6A levels in both Mettl3 KD and Mettl14 KD versus control cells (Fig. 1c). We then used liquid chromatography–tandem mass spectrometry to quantify m^6A/A ratios and observed a 60–70% decrease in m^6A levels in each KD line relative to controls (Fig. 1d), suggesting that both proteins mediate m^6A formation *in vivo*. mESCs expressing additional shRNAs targeting *Mettl3* or *Mettl14* were generated to control for shRNA off-target effects (Supplementary Fig. 1A) and similarly decreased m^6A levels were detected in all KD clones (Supplementary Fig. 1B). We then carried out a direct methylation assay by incubating an RNA probe exhibiting four repeats of the canonical m^6A methylation motif (GGACU) with equal amounts of luciferase, Mettl3 and/or Mettl14 proteins (Fig. 1e and Supplementary Fig. 1C) purified from HEK293 cells in the presence of [^{3}H]SAM and assessed [^{3}H]methyl transfer. The RNA probe incubated with control luciferase protein showed no increase in [^{3}H] levels. However, 1.5-, 3.5- and >27-fold increases in [^{3}H] levels were detected in probes incubated with Mettl3, Mettl14 and Mettl3+Mettl14 (Fig. 1f), respectively. Thin-layer chromatography analysis confirmed that methylated nucleotides were m^6A (Fig. 1g and Supplementary Fig. 1D). To exclude the possibility that the enzymatic activity was due to promiscuously co-purified mammalian proteins, we performed methylation assays using proteins purified from baculovirus-infected Sf9 insect cells. We found Mettl3 and Mettl14 difficult to purify alone but they were easily co-purified when co-expressed. As shown in Supplementary Fig. 1E, Mettl3 was specifically pulled down by Mettl14 but not luciferase, suggesting a strong interaction between

[1]Tumor Initiation and Maintenance Program, NCI-designated Cancer Center, Sanford Burnham Medical Research Institute, La Jolla, California 92037, USA. [2]Department of Computer Science, The Donnelly Centre, University of Toronto, Toronto M5S 3G4, Canada. [3]Department of Molecular Genetics, Donnelly Centre for Cellular and Biomolecular Research, Banting and Best Department of Medical Research, University of Toronto, Toronto M5S 3G4, Canada.
[4]Correspondence should be addressed to J.C.Z. (e-mail: czhao@sanfordburnham.org)

Received 24 May 2013; accepted 29 November 2013; published online 7 January 2014; DOI: 10.1038/ncb2902

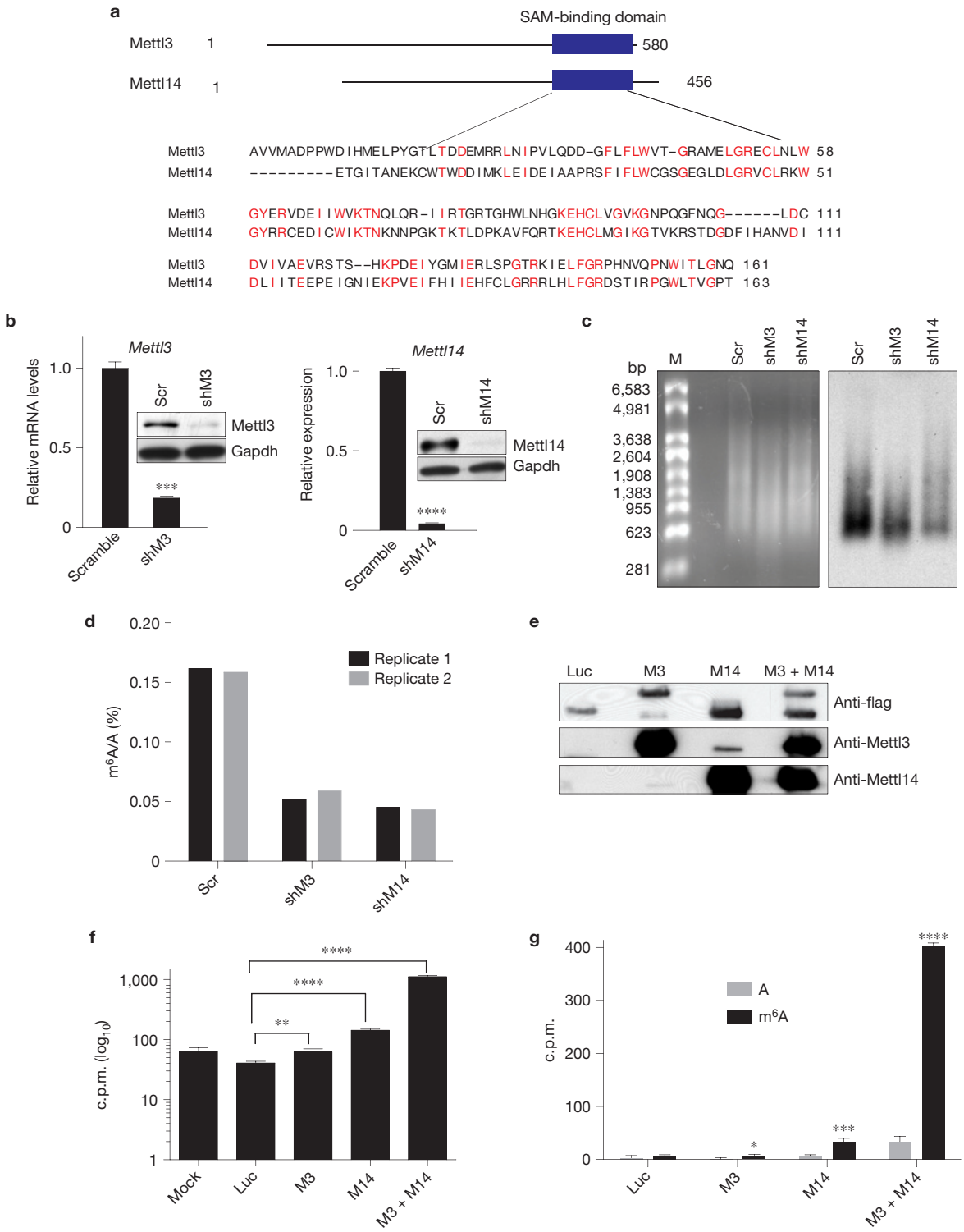

Figure 1 *Mettl3* and *Mettl14* are required for m^{6}A formation *in vitro* and *in vivo*. (**a**) Schematic drawing showing predicted MTase domains of mouse Mettl3 (Accession: NP_062695.2) and Mettl14 (Accession: NP_964000.2) proteins. Numbers represent amino acid numbers. (**b**) RT–qPCR (left) and western blot (right) showing *Mettl3* (left panel) and *Mettl14* (right panel) expression in mESC clones stably expressing shRNAs targeting each. Gapdh serves as a loading control in the western blot. Scr: scramble; shM3, shRNA against *Mettl3*; shM14, shRNA against *Mettl14*. The original gel is shown in Supplementary Fig. 5. (**c**) Ethidium bromide staining (left panel) and m^{6}A immunoblot (right panel) of DNA-free, rRNA-free Poly(A)+ RNA from Mettl3 KD, Mettl14 KD and control cells. (**d**) Measurement of percentage of m^{6}A/A ratio by MS. (**e**) Flag, Mettl3 or Mettl14 western immunoblots of proteins purified from lysates of HEK293 cells overexpressing flag-tagged Mettl3, Mettl14, or luciferase using M2 beads. Luc, luciferase; M3, Mettl3; M14, Mettl14. The original gel is shown in Supplementary Fig. 5. (**f**) c.p.m. of RNA probes extracted after an *in vitro* methylation assay. (**g**) c.p.m. of excised m^{6}A spots from digested RNA probes used in the methylation assay. Error bars in **b**,**f**,**g** represent means ± s.e.m. from three separate experiments, except M3 in **g** where $n = 7$. One-tailed Student's *t*-test, $^{*}P < 0.05$, $^{**}P < 0.01$, $^{***}P < 0.001$, $^{****}P < 0.0001$ versus scramble control. Scr: scramble control.

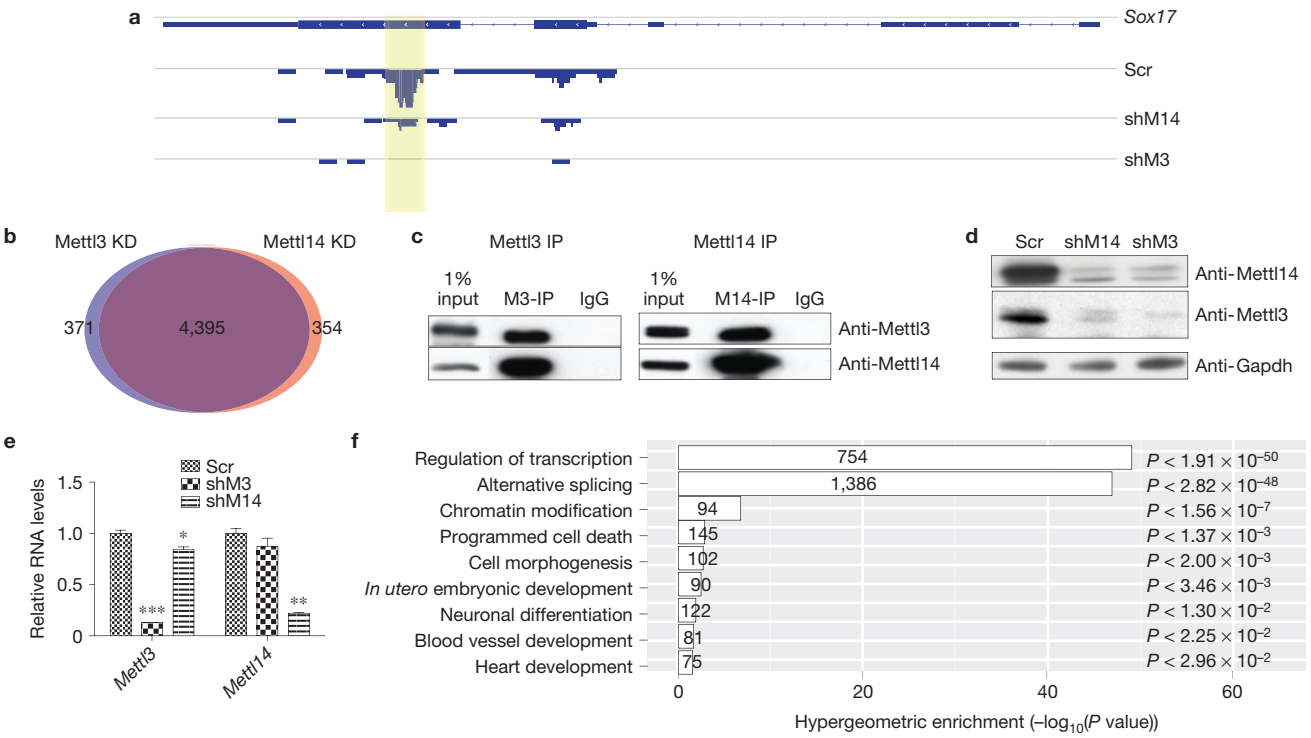

Figure 2 Mettl3 and Mettl14 interact and regulate each other's stability. (**a**) meRIP-seq analysis of a Sox17 transcript showing loss of m^{6}A methylation in both Mettl3 KD and Mettl14 KD cells. Yellow highlighting, peak location. Scr: scramble; shM3, shRNA against *Mettl3*; shM14, shRNA against *Mettl14*. (**b**) Venn diagram showing overlap of Mettl3 and *Mettl14* targets. (**c**) Mettl3 or Mettl14 western immunoblots of endogenous proteins co-immunoprecipitated using antibodies against Mettl3 or Mettl14, or IgG in mESC lysates. M3, Mettl3; M14, Mettl14. The original gel is shown in Supplementary Fig. 5. (**d**) Western blot analysis of Mettl3 and Mettl14 protein levels in Mettl3 KD and Mettl14 KD mESCs, respectively. The original gel is shown in Supplementary Fig. 5. (**e**) RT–qPCR analysis of Mettl3 and Mettl14 RNA levels in Mettl3 KD and Mettl14 KD mESCs, respectively. (**f**) GO analysis of 4,395 shared Mettl3 and Mettl14 targets. Error bars in **e** represent means ± s.e.m. from three separate experiments. One-tailed Student's *t*-test, $^*P < 0.05$, $^{**}P < 0.01$, $^{***}P < 0.001$ versus scramble control. Scr: scramble.

Mettl3 and Mettl14. Importantly, Mettl3 + Mettl14 exhibited high m^{6}A MTase activity (Supplementary Fig. 1F,G), demonstrating that MTase activities detected from HEK293 purified proteins are indeed from Mettl proteins. To further assess specificity, we performed KD analysis targeting *Mettl4*, a gene of the *Mettl3* and *Mettl14* superfamily, and detected no change in m^{6}A levels despite high KD efficiency (Supplementary Fig. 1H,I). These studies show that both Mettl3 and Mettl14 exhibit *in vitro* and *in vivo* MTase activity and suggest that they function synergistically.

We next performed a genome-wide search for RNA substrates showing decreased m^{6}A methylation in KD mESCs by coupling m^{6}A immunoprecipitation with high-throughput sequencing[6,7] (meRIP-seq). Twelve libraries, including replicates of a pair of input and meRIP samples from scramble controls, Mettl3 KD and Mettl14 KD cells, were sequenced. Approximately 38–55 million reads were generated for each type of library and high Pearson correlation coefficients ($R \geq 0.97$) were obtained among replicates, suggesting high library reproducibility. There are 3.8–6.7 million distinct reads uniquely aligned to the mouse mm10 reference genome. These reads were used to detect m^{6}A sites, which were identified by MACS peak-calling software. A stringent cutoff threshold for false discovery rate (FDR) of <10% was used to obtain high-confidence peaks. After combining replicate libraries, 8,645, 6,667 and 6,159 high-confidence peaks from scramble, Mettl3 KD and Mettl14 KD cells, respectively, remained for analysis. Overall, 4,766 genes in Mettl3 KD and 4,749 in Mettl14 KD cells showed significantly decreased transcript m^{6}A levels relative to controls. For example, the Sox17 mRNA methylation peak was detected only in the scramble control but not in Mettl3 or Mettl14 KD cells (Fig. 2a and Supplementary Table 1). Interestingly, Mettl3 and Mettl14 targets overlapped substantially (Fig. 2b), supporting our hypothesis that they synergize. To examine potential interaction *in vivo*, we performed co-immunoprecipitation of both endogenous and flag-tagged Mettl3 and Mettl14. All experiments demonstrated robust and specific interaction of both proteins (Fig. 2c and Supplementary Fig. 2A). To determine whether Mettl3 or Mettl14 homodimerize, flag- and HA-tagged Mettl3 or Mettl14 were co-expressed in HEK293 cells. No HA–Mettl3 was pulled down by flag–Mettl3 (Supplementary Fig. 2B), indicating that Mettl3 does not homodimerize. Similar results were observed for Mettl14 (Supplementary Fig. 2B). We then investigated whether these proteins regulated each other's expression. Strikingly, we observed an almost total loss of Mettl3 protein in Mettl14 KD cells (Fig. 2d), despite a small decrease in Mettl3 RNA (Fig. 2e). Comparable results were observed for Mettl14 protein and RNA in Mettl3 KD cells (Fig. 2d,e), suggesting that Mettl3 and Mettl14 stabilize each other at the protein levels. Finally, GO analysis indicated that Mettl3 and Mettl14 targets regulate transcription, RNA splicing, chromatin modification, programmed cell death and cell fate determination (Fig. 2f). Overall, these results suggest that Mettl3 and Mettl14 regulate m^{6}A modification

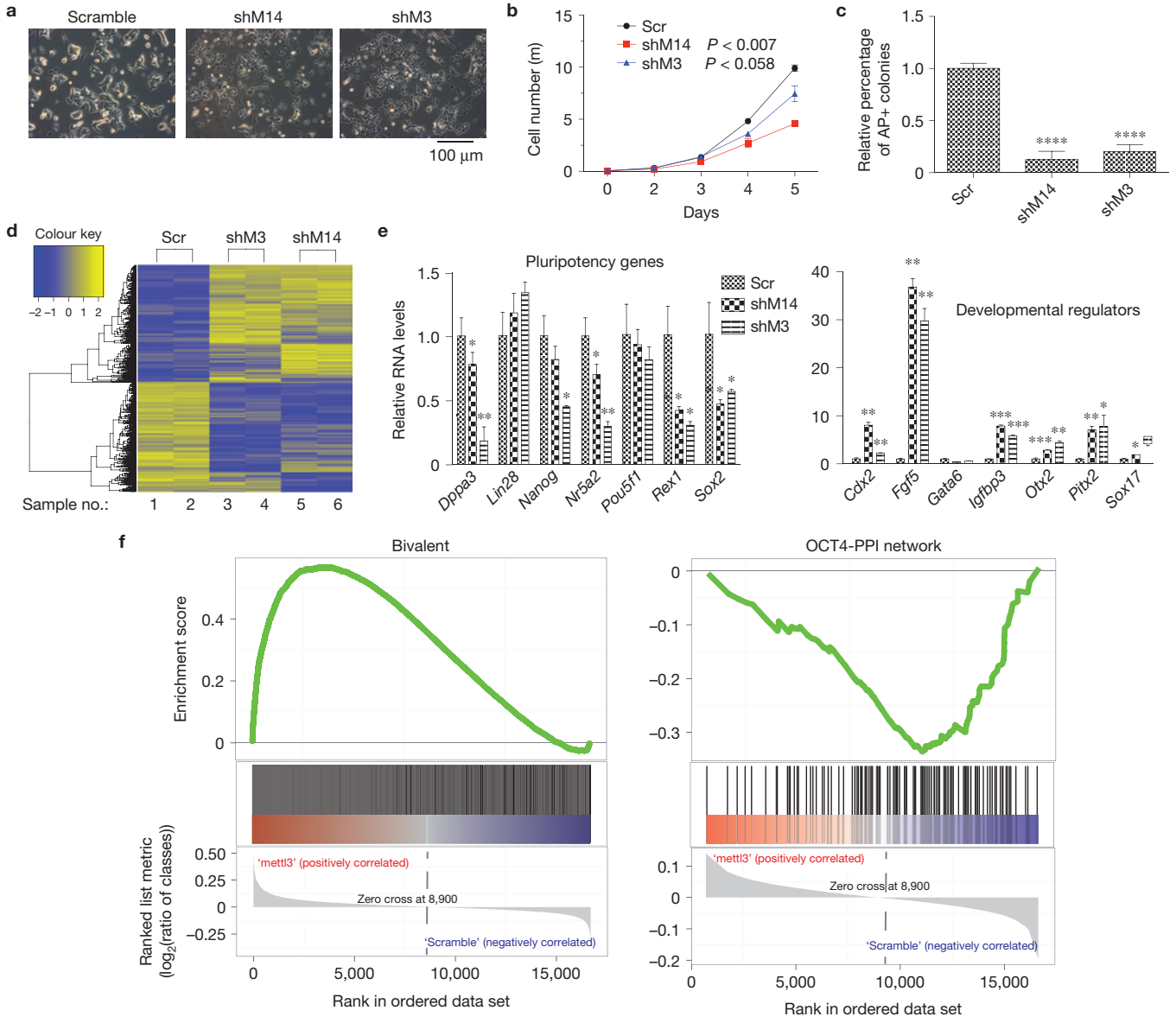

Figure 3 *Mettl3* or *Mettl14* KD mESCs lose self-renewal capability. (**a**) Phase-contrast microscopy showing colony morphology of KD versus control mESC cells. Scr: scramble; shM3, shRNA against *Mettl3*; shM14, shRNA against *Mettl14*. (**b**) Growth curve assessing cell proliferation kinetics of KD versus control cells. *P* values are generated by two-way analysis of variance. (**c**) Quantification of AP-positive colonies. (**d**) Heat map analysis based on microarray comparison of gene expression in KD and control cells. (**e**) RT–qPCR analysis of pluripotency (left) and differentiation (right) genes in KD versus control cells. (**f**) GSEA analysis on enrichment of developmental regulators (left) and pluripotency-related genes (right) in Mettl3 KD versus control cells. An FDR of <0.178 was calculated for bivalent genes and FDR < 0 for pluripotency-related genes. Note that FDR < 0.25 is statistically significant for GSEA analysis: www.broadinstitute.org/gsea/doc/GSEAUserGuideFrame.html. Error bars in **b**,**c** and **e** represent mean ± s.e.m. from three separate experiments. One-tailed Student's *t*-test, $^{*}P < 0.05$, $^{**}P < 0.01$, $^{***}P < 0.001$, $^{****}P < 0.0001$ versus scramble control. Scr: scramble.

of a significant number of mRNAs in mammalian cells, possibly by participating in a complex.

Phenotypically, Mettl3 or Mettl14 KD mESC colonies were flatter and less compact than control colonies (Fig. 3a and Supplementary Fig. 3A), and had a decreased cell proliferation rate (Fig. 3b). Alkaline phosphatase (AP) staining showed that only 20–30% of mESC colonies were AP-positive in KD cells relative to scramble controls (Fig. 3c and Supplementary Fig. 3B). More quantitative fluorescence-activated cell sorting analysis of AP-positive cells showed that 50.8% of control cells exhibited high AP levels, whereas 32.2 and 37.7% of Mettl3 KD and Mettl14 KD cells, respectively, showed high AP levels. SSEA-1 fluorescence-activated cell sorting analysis revealed no difference between KD (99.7 and 96.5% for *Mettl3* and *Mettl14*, respectively) and control (99.3%) cells, indicating that KD cells differ from terminal differentiated cells and maintain some stem cell features. To understand these outcomes at the molecular level, we carried out microarray analysis of Mettl3 KD and Mettl14 KD mESCs and found that both shared gene expression profiles distinct from

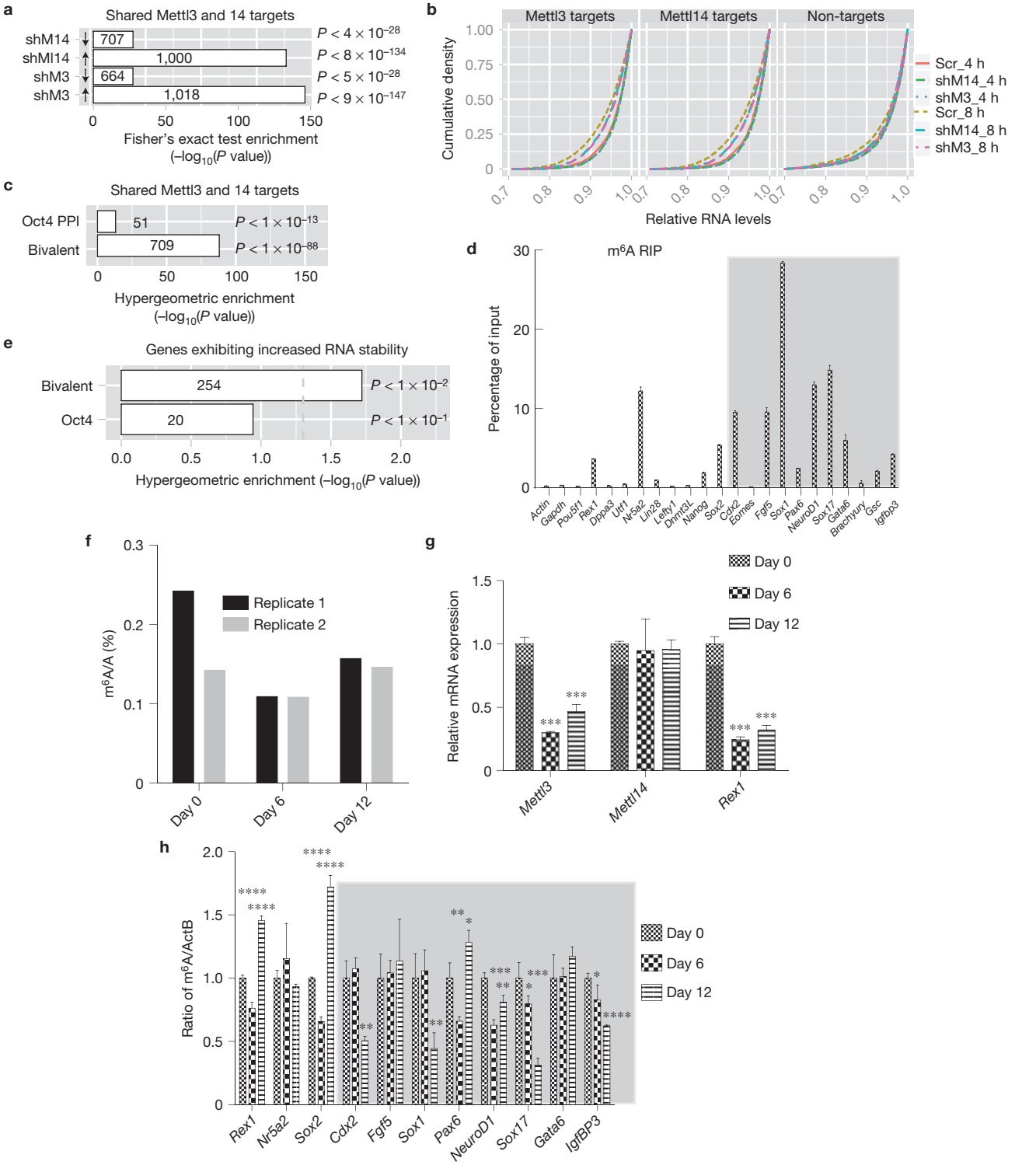

Figure 4 m^{6}A modification regulates mRNA stability. (**a**) Enrichment of upregulated or downregulated Mettl3 and Mettl14 targets in KD versus control cells. Arrows indicate upregulation or downregulation of gene expression. Scr: scramble; shM3, shRNA against *Mettl3*; shM14, shRNA against *Mettl14*. (**b**) Comparison of cumulative transcript abundance in cells treated with ActD for 0, 4 and or 8 h by microarray analysis. RNAs from 0 h serve as base-line. Kolmogorov–Smirnov test, $P < 2.2 \times 10^{-16}$ comparing the changes in relative RNA levels from 4 to 8 h between Mettl targets and non-targets in both Mettl3 KD and Mettl14 KD cells. (**c**) Enrichment of bivalent and pluripotency (Oct4 PPI) genes in shared Mettl3 and Mettl14 targets. (**d**) meRIP-qPCR of specific bivalent and pluripotency genes (grey area). (**e**) Enrichment of Mettl3 and Mettl14 targets showing increased RNA stability in KD cells among bivalent and pluripotency genes. (**f**) Measurement of a percentage of m^{6}A/A ratio by MS in undifferentiated (day 0), day6, and day 12 differentiated mESCs. (**g**) RT–qPCR of *Mettl3*, *Mettl14* and *Rex1* expression in undifferentiated and differentiated mESCs. (**h**) meRIP-qPCR of specific bivalent (grey area) and pluripotency genes in mESCs during differentiation. Error bars in **d**,**g**,**h** represent means ± s.e.m. from three separate experiments. One-tailed Student's *t*-test, $^{*}P < 0.05$, $^{**}P < 0.01$, $^{***}P < 0.001$, $^{****}P < 0.0001$ versus scramble control. Scr: scramble.

control cells (Fig. 3d). Analysis by quantitative PCR with reverse transcription (RT–qPCR) indicated that most pluripotency factors were downregulated in Mettl3 or Mettl14 KD cells relative to controls (left panels of Fig. 3e and Supplementary Fig. 3C), whereas some developmental regulators were significantly upregulated (right panels of Fig. 3e and Supplementary Fig. 3C). Similar results were obtained from mESCs transfected for 48 h with short interfering RNAs (siRNAs) targeting either *Mettl3* or *Mettl14* genes (Supplementary Fig. 3D). To expand these observations, genome-wide, gene-set enrichment analysis (GSEA) of pluripotency-related genes and developmental regulators was performed assessing differential gene expression levels in KD versus control cells. Developmental regulators were defined as the ~2,800 bivalent genes whose promoters exhibit both eu- and hetero-chromatin markers in mESCs (ref. 13), and 145 genes present in the Oct4-centred protein–protein interaction (PPI) network were used as pluripotency-related genes[14]. GSEA analysis showed enrichment of developmental regulators in both Mettl3 and Mettl14 KD versus control cells (left panels of Fig. 3f and Supplementary Fig. 3E), whereas pluripotency-related genes showed negative enrichment (right panels of Fig. 3f and Supplementary Fig. 3E). Taken together, these studies suggest that m^{6}A methylation is essential to maintain mESCs at their ground state.

m^{6}A is highly enriched near stop codons[6,7]. Thus, we conducted ^{35}S-pulse labelling in KD and control mESCs to determine whether depletion of modification impaired protein synthesis and detected no significant changes (Supplementary Fig. 4A,B). However, analysis of potential correlation between RNA methylation and gene expression levels indicated that loss of m^{6}A methylation following Mettl3 KD or Mettl14 KD was more significantly associated with gene upregulation than downregulation (Fig. 4a and Supplementary Fig. 4C). Multiple cellular mechanisms can contribute to increased RNA levels. As m^{6}A is an internal modification that is enriched at the 3′-UTR (refs 6,7), we investigated whether m^{6}A affects the mRNA decay rate by measuring RNA levels from actinomycin D (ActD)-treated scramble and KD mESCs. Significantly, Mettl targets showed a ~23% increase in the maximum cumulative RNA stability in KD cells when compared with the controls (Fig. 4b, left and mid-panels, and Supplementary Table 2) from 4 to 8 h after ActD treatment, in contrast to only 9% for the non-targets (Fig. 4b, right panel, and Supplementary Table 2), suggesting that m^{6}A modification accelerates transcript decay.

Next we examined whether developmental regulators or pluripotency-related genes are subject to m^{6}A regulation. Enrichment analysis showed that when compared with pluripotency-related genes, developmental regulators were much more significantly enriched in Mettl3 and Mettl14 targets (Fig. 4c). meRIP RT–qPCR of both gene subclasses confirmed that transcripts of many developmental regulators were more highly enriched in m^{6}A methylation than were transcripts encoding housekeeping genes (such as *ActB* or *Gapdh*) or the pluripotency factors (such as *Pou5f1* or *Nanog*; Fig. 4d). Bivalent genes identified as Mettl3 or Mettl14 targets also showed a more significant increase in RNA stability than did pluripotency genes following KD of either protein (Fig. 4e), suggesting that m^{6}A methylation destabilizes developmental regulators. To further understand the dynamics of m^{6}A modification, we measured m^{6}A levels during mESC differentiation. Cells at day 6 or 12 of differentiation showed overall levels of m^{6}A (Fig. 4f) or *Mettl14* expression (Fig. 4g) comparable to undifferentiated mESCs, although we detected a moderate decrease in *Mettl3* expression in differentiated cells (Fig. 4g). Interestingly, gene-specific meRIP-qPCR showed significantly decreased m^{6}A levels in 5 of 8 developmental regulators examined in day 12 cells (Fig. 4h, grey area). In contrast, all 3 pluripotency-related genes showed unchanged or increased m^{6}A levels (Fig. 4h). These data indicate that developmental regulators are subject to m^{6}A regulation in mESCs.

To assess the molecular mechanisms underlying m^{6}A-methylation-mediated RNA decay, we focused on the well-established RNA stabilizer protein HuR (refs 15,16), which binds to the U-rich regions at the 3′-UTR of thousands of transcripts[17,18]. Enrichment analysis suggested that Mettl targets exhibiting HuR-binding sites showed significantly increased RNA stability (Fig. 5a) relative to those without HuR sites. We then investigated whether the presence of m^{6}A affects HuR binding to RNA. To do so, we incubated purified HuR protein (Supplementary Fig. 4D) with fragmented mRNA extracted from scramble, Mettl3 KD and Mettl14 KD cells (Fig. 5b, left panel) and performed RNA electrophoretic mobility shift assay analyses. We observed increased HuR binding to demethylated mRNA extracted from KD when compared with control cells (Fig. 5b, mid-panels). However, work reported in ref. 7 indicated that HuR interacts with an RNA probe containing m^{6}A *in vitro*. To assess this potential discrepancy, we examined the ~60-base-pair (bp) RNA probe used in that study in which m^{6}A is immediately adjacent to the HuR-binding site. We reasoned that endogenous m^{6}A and HuR sites may not always co-localize because the predicted RNA motifs of m^{6}A and HuR binding sites differ substantially and postulate that the spacing of HuR and m^{6}A sites may affect their interaction. Thus, we designed RNA probes with no spacer (Fig. 5c, RNA probes 0A and 0m^{6}A) or a 12-nucleotide (nt) spacer (Fig. 5c, RNA probes 12A and 12m^{6}A) between A/m^{6}A and HuR sites. Consistent with ref. 7, we observed significantly increased HuR binding to the 0m^{6}A versus 0A RNA probes (Fig. 5b, right panel). In contrast, we observed moderately decreased HuR binding in the presence of the 12-nt spacer (Fig. 5b, right panel), suggesting that spatial constraints govern m^{6}A and HuR binding.

To analyse potential negative interaction between HuR and m^{6}A *in vivo*, we chose three representative genes for validation: *Pou5f1*, *Otx2* and *Igfbp3*. Pou5f1 transcripts lack m^{6}A, whereas bivalent Otx2 and Igfbp3 are Mettl3 and Mettl14 targets that showed increased expression in KD cells (Fig. 3e and Supplementary Fig. 3C). The Igfbp3 3′-UTR, however, exhibits a HuR-binding motif, whereas that of Otx2 does not. Assessment of the m^{6}A methylation status of Otx2 and Igfbp3 showed that both transcripts were demethylated in Mettl KD cells (Supplementary Fig. 4E). RIP analysis indicated increased HuR binding at the Igfbp3 3′-UTR in Mettl3 or Mettl14 KD cells, but not of Otx2 or Pou5f1 (Fig. 5d), suggesting that demethylation accompanies HuR binding. Importantly, increased HuR binding accompanied increased stability of Igfbp3 RNA but not of Otx2 and Pou5f1 in KD cells (Fig. 5e). To determine whether HuR mediated that increased stability, we first confirmed that we could target *HuR* efficiently with siRNA in Mettl3 or Mettl14 KD cells (Supplementary Fig. 4F). We then measured Igfbp3 RNA stability in these cells in the absence of HuR and observed that stability was restored to control levels (Fig. 5e). This result was confirmed by specifically decreased *Igfbp3* expression in mESCs depleted of HuR (Fig. 5f). Overall, our *in vivo* analysis suggests that loss of m^{6}A methylation enhances HuR RNA binding to increase RNA stability.

HuR binding reportedly increases RNA stability by blocking microRNA targeting[15,16]. *Igfbp3*, for example, is a direct target of

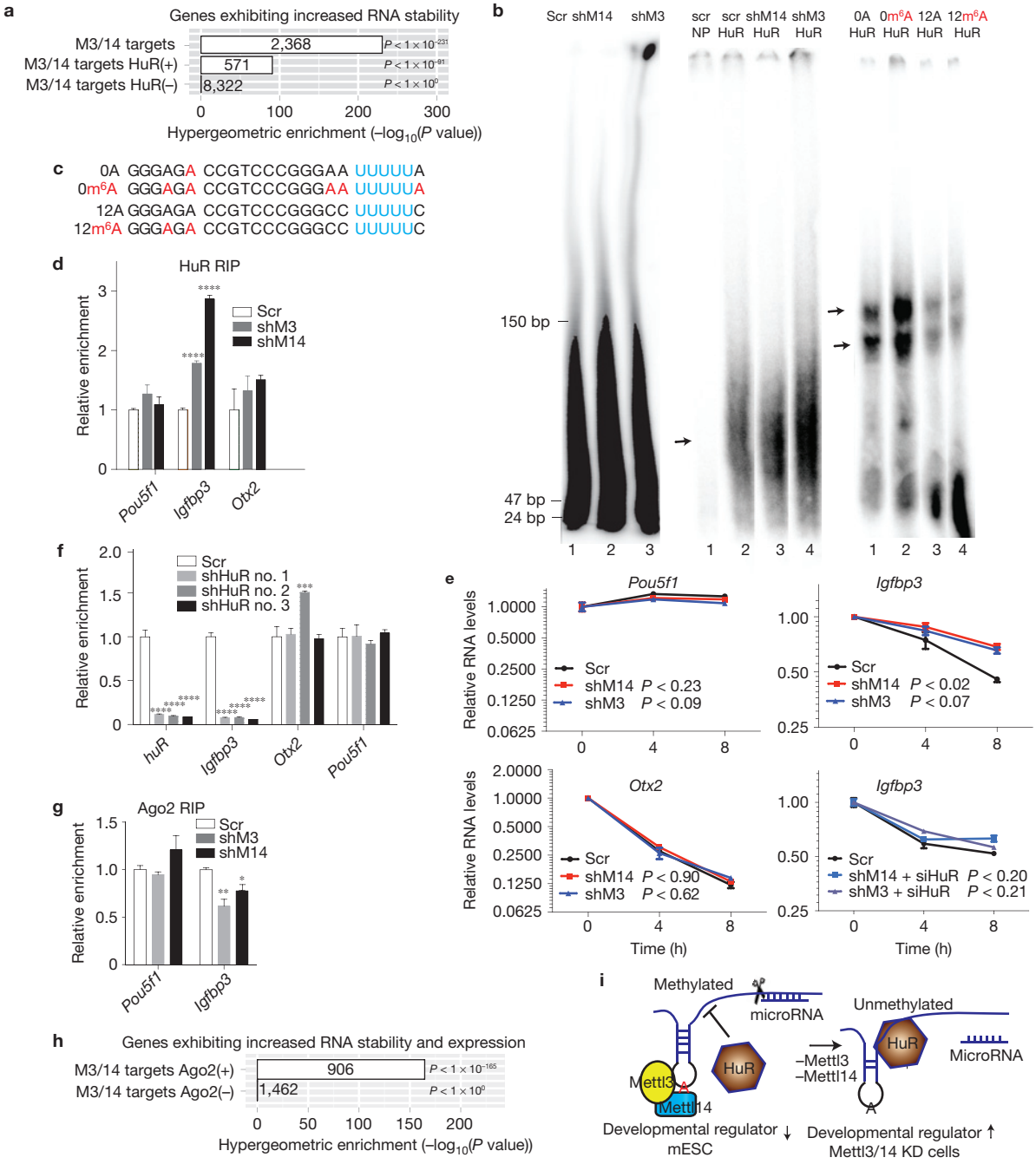

Figure 5 The HuR-microRNA pathway functions in m^{6}A-methylation-mediated RNA stability. (**a**) Enrichment of genes showing increased RNA stability following Mettl3 or Mettl14 KD among all shared Mettl3 and Mettl14 targets and among targets with and without canonical HuR-binding sites in their 3′-UTR regions. M3, Mettl3; M14, Mettl14. (**b**) Left panel, denaturing PAGE showing the size of fragmented, DNAse-treated, rRNA-free mRNAs extracted from scramble and KD cells; middle panel, non-denaturing PAGE showing differential binding of HuR to RNAs probes from left panel. Scr: scramble control, shM14, shRNA against *Mettl14*, shM3, shRNA against *Mettl3*. NP: no protein added. Right panel, non-denaturing PAGE showing differential binding of HuR to RNA probes in **c**. (**c**) RNA probes with the canonical UUUUU HuR-binding site located either next to A (0A) or m^{6}A (0m^{6}A) or separated by a 12-nucleotide spacer (12A and 12m^{6}A). (**d**) HuR RIP-qPCR of *Pou5f1*, *Igfbp3* and *Otx2* from KD versus control cells. (**e**) RT–qPCR of *Pou5f1*, *Igfbp3* and *Otx2* in ActD-treated KD cells. In the case of *Igfbp3*, cells are also treated with and without siRNA targeting *HuR*. *P* values are generated using two-way analysis of variance. (**f**) RT–qPCR of HuR, Igfbp3, Otx2 and Pou5f1 in mESCs with depleted HuR. shHuR no. 1–3: shRNAs against *HuR*. (**g**) Ago2 RIP-qPCR of Igfbp3 and Pou5f1 RNAs from KD versus control cells. (**h**) Enrichment of genes showing increased RNA stability and expression among shared Mettl3 and Mettl14 targets. Targets are classified by whether they exhibit Ago2 binding sites. (**i**) Model: in wild-type mESCs, Mettl3 and Mettl14 methylate RNA synergistically and m^{6}A methylation on some transcripts, particularly those encoding developmental regulators, blocks HuR binding, resulting in transcript destabilization. In Mettl3 and Mettl14 KD cells, loss of m^{6}A allows HuR–mRNA interaction and attenuation of microRNA targeting, enhancing stability of transcripts especially those encoding developmental regulators, and promoting loss of the mESC ground state. A potentially methylated A is shown in red. Error bars in **d**–**g** represent means ± s.e.m. from three separate experiments. One-tailed Student's *t*-test, $^*P < 0.05$, $^{**}P < 0.01$, $^{***}P < 0.001$, $^{****}P < 0.0001$ versus scramble control. Scr: scramble.

several microRNAs[19,20]. Therefore, we carried out RIP with argonaute 2 (Ago2), a key factor of the RNA-induced silencing complex, in Mettl3 or Mettl14 KD cells. We observed a ~25–40% decrease in Ago2 binding to the Igfbp3 3′-UTR, but little change to Pou5f1, which is not a methylation target and exhibits equivalent HuR binding in KD versus control cells (Fig. 5g). To understand whether this mechanism applies to other RNAs, we evaluated Mettl3 or Mettl14 targets that show increased RNA stability and expression in relation to Ago2-bound mRNAs in KD versus control mESCs, as defined by a previous CLIP-seq (cross-linking immunoprecipitation coupled with high-throughput sequencing) study[21]. Interestingly, we observed specific enrichment of Ago2-bound Mettl3/14 targets (Fig. 5h) but not targets lacking Ago2 binding. These results suggest that the HuR/microRNA pathway mediates m^{6}A-regulated RNA stability.

We propose a model in which the presence of m^{6}A methylation on some transcripts in mESCs, particularly those encoding developmental regulators, blocks HuR binding and destabilizes them, thereby maintaining the mESC ground state (Fig. 5i). Our work suggests that m^{6}A methylation is an essential RNA regulatory mechanism in mammalian cells. □

METHODS

Methods and any associated references are available in the online version of the paper.

Note: Supplementary Information is available in the online version of the paper

ACKNOWLEDGEMENTS

We thank M. Wilkinson and all members of his laboratory for many valuable discussions; the Mass Spectrometry, Metabolomics, and Proteomics Facility at the University of Illinois at Chicago for measuring m^{6}A/A ratios; S. S. Govindarajan from the Analytical Genomics core facility at the Sanford Burnham Medical Institute (Lake Nona) for performing the microarray analysis; and P. Ordoukhanian and S. R. Head from the Scripps Research Institute for high-throughput sequencing analysis. This work is supported by a CIRM Training Grant TG2-01162 (Y.W.), an AACR-Aflac, Career Development Award for Pediatric Cancer Research 12-20-10-ZHAO (J.C.Z.), the Ontario Research Fund - Global Leader (Round 2) and Natural Sciences and Engineering Research Council (NSERC; Z.Z.), and an NSERC Canada Graduate Scholarship and Ontario Graduate Scholarship (Y.L.). M.D.P. is an American Cancer Society Research Scholar (RSG-11-224-01-DMC). Z.Z. would like to dedicate this paper to the memory of S.Z.

AUTHOR CONTRIBUTIONS

Y.W. generated Mettl3 and Mettl14 KD mESC lines, and using these lines, designed, performed and analysed most experiments, except meRIP, RIPs and EMSAs. meRIP, RIPs and EMSAs were performed by Y.W. and J.C.Z. Y.L. performed all bioinformatics analysis under the supervision of Z.Z. J.I.T. and M.D.P. purified luciferase, Mettl3 and/or Mettl14 proteins from baculovirus-infected Sf9 insect cells. J.C.Z. formulated, analysed and directed the study and wrote the paper.

COMPETING FINANCIAL INTERESTS

The authors declare no competing financial interests.

Published online at www.nature.com/doifinder/10.1038/ncb2902
Reprints and permissions information is available online at www.nature.com/reprints

1. Jia, G., Fu, Y. & He, C. Reversible RNA adenosine methylation in biological regulation. *Trends Genet.* **29,** 108–115 (2013).
2. Clancy, M. J., Shambaugh, M. E., Timpte, C. S. & Bokar, J. A. Induction of sporulation in *Saccharomyces cerevisiae* leads to the formation of N6-methyladenosine in mRNA: a potential mechanism for the activity of the IME4 gene. *Nucleic Acids Res.* **30,** 4509–4518 (2002).
3. Agarwala, S. D., Blitzblau, H. G., Hochwagen, A. & Fink, G. R. RNA methylation by the MIS complex regulates a cell fate decision in yeast. *PLoS Genet.* **8,** e1002732 (2012).
4. Zhong, S. *et al.* MTA is an *Arabidopsis* messenger RNA adenosine methylase and interacts with a homolog of a sex-specific splicing factor. *Plant Cell* **20,** 1278–1288 (2008).
5. Bodi, Z. *et al.* Adenosine methylation in *Arabidopsis* mRNA is associated with the 3′ end and reduced levels cause developmental defects. *Front. Plant Sci.* **3,** 1–10 (2012).
6. Meyer, K. D. *et al.* Comprehensive analysis of mRNA methylation reveals enrichment in 3′ UTRs and near stop codons. *Cell* **149,** 1635–1646 (2012).
7. Dominissini, D. *et al.* Topology of the human and mouse m6A RNA methylomes revealed by m6A-seq. *Nature* **485,** 201–206 (2012).
8. Zheng, G. *et al.* ALKBH5 is a mammalian RNA demethylase that impacts RNA metabolism and mouse fertility. *Mol. Cell* **49,** 18–29 (2013).
9. Jia, G. *et al.* N6-methyladenosine in nuclear RNA is a major substrate of the obesity-associated FTO. *Nat. Chem. Biol.* **7,** 885–887 (2011).
10. Bokar, J. A., Shambaugh, M. E., Polayes, D., Matera, A. G. & Rottman, F. M. Purification and cDNA cloning of the AdoMet-binding subunit of the human mRNA (N6-adenosine)-methyltransferase. *RNA* **3,** 1233–1247 (1997).
11. Bujnicki, J. M., Feder, M., Radlinska, M. & Blumenthal, R. M. Structure prediction and phylogenetic analysis of a functionally diverse family of proteins homologous to the MT-A70 subunit of the human mRNA:m(6)A methyltransferase. *J. Mol. Evol.* **55,** 431–444 (2002).
12. Petrossian, T. C. & Clarke, S. G. Uncovering the human methyltransferasome. *Mol. Cell. Proteom.* **10,** M110.000976-1-12 (2011).
13. Ku, M. *et al.* Genomewide analysis of PRC1 and PRC2 occupancy identifies two classes of bivalent domains. *PLoS Genet.* **4,** e1000242 (2008).
14. van den Berg, D. L. *et al.* An Oct4-centered protein interaction network in embryonic stem cells. *Cell Stem Cell* **6,** 369–381 (2010).
15. Srikantan, S., Tominaga, K. & Gorospe, M. Functional interplay between RNA-binding protein HuR and microRNAs. *Curr. Protein Peptide Sci.* **13,** 372–379 (2012).
16. Kundu, P., Fabian, M. R., Sonenberg, N., Bhattacharyya, S. N. & Filipowicz, W. HuR protein attenuates miRNA-mediated repression by promoting miRISC dissociation from the target RNA. *Nucleic Acids Res.* **40,** 5088–5100 (2012).
17. Kishore, S. *et al.* A quantitative analysis of CLIP methods for identifying binding sites of RNA-binding proteins. *Nat. Methods* **8,** 559–564 (2011).
18. Lebedeva, S. *et al.* Transcriptome-wide analysis of regulatory interactions of the RNA-binding protein HuR. *Mol. Cell* **43,** 340–352 (2011).
19. Le, M. T. *et al.* Conserved regulation of p53 network dosage by microRNA-125b occurs through evolving miRNA-target gene pairs. *PLoS Genet.* **7,** e1002242 (2011).
20. Lu, L., Katsaros, D., de la Longrais, I. A., Sochirca, O. & Yu, H. Hypermethylation of let-7a-3 in epithelial ovarian cancer is associated with low insulin-like growth factor-II expression and favorable prognosis. *Cancer Res.* **67,** 10117–10122 (2007).
21. Leung, A. K. *et al.* Genome-wide identification of Ago2 binding sites from mouse embryonic stem cells with and without mature microRNAs. *Nat. Struct. Mol. Biol.* **18,** 237–244 (2011).

METHODS

Cell lines. J1 mouse embryonic stem cells (mESCs) were cultured as described previously[22]. These cells are free of mycoplasma when tested with a Mycoplasma Detection Kit (Lonza). Cells were differentiated by culturing them in suspension with LIF-depleted medium for four days to form embryonic bodies, followed by seeding embryonic bodies on 0.2% gelatin-coated plates and collecting them at different time points. Lentiviral constructs harbouring shRNAs against Mettl3 or Mettl14 were purchased from Sigma-Aldrich (see the shRNA sequences section for details). Stable mESC knockdown (KD) lines were generated using standard viral infection and puromycin selection (2 μg ml^{-1}).

Purification of mRNA. Total RNA was isolated using TRIZOL (Invitrogen) and treated with DNaseI (Roche). Polyadenylated mRNA was purified using GenElute mRNA Miniprep Kit (Sigma-Aldrich) and residual ribosomal RNA was depleted with RiboMinus Eukaryote System v2 (Life Technologies).

Immunoblot detection of m^{6}A. Purified mRNA (250 ng) was separated on a 1.4% denaturing agarose gels and transferred to a nylon membrane (Millipore). After crosslinking with an ultraviolet crosslinker (Spectroline), the membrane was blocked with 5% non-fat milk in TBST and then incubated with antibody against m^{6}A (Synaptic Systems, catalogue number 202 003, 1:5,000) and then an HRP-conjugated antibody against rabbit IgG. After incubation with the Immobilon Western Chemiluminescent HRP Substrate (Millipore), the membrane was exposed to autoradiography film (Kodak).

Determination of the m^{6}A/A ratio by liquid chromatography–tandem mass spectrometry. DNA- and rRNA-free PolyA RNAs were prepared and liquid chromatography–tandem mass spectrometry was carried out on blinded samples at the Mass Spectrometry, Metabolomics, and Proteomics Facility at the University of Illinois at Chicago, as described previously[9].

Protein purification from HEK293 cells. HEK293 cells were transiently transfected with constructs encoding flag-tagged luciferase, Mettl3, Mettl14, Mettl3 + Mettl14 and HuR. Whole-cell lysates were collected 48 h after transfection and proteins were purified with anti-flag M2 Magnetic Beads (Sigma-Aldrich, catalogue number M8823) following the manufacturer's protocol.

m^{6}A methylation assay. A 5′-GGACUGGACUGGACUGGACU-3′ RNA probe was synthesized by *in vitro* transcription using an AmpliScribe T7-*Flash* Transcription Kit (Epicentre). The reaction mix contained 15 mM HEPES, 1 mM dithiothreitol, 4% glycerol, 50 mM KCl, 50 mM NaCl, 1 mM $MgCl_2$, 1.5 μCi of adenosyl-L-methionine, [methyl-3H]SAM, 0.5 μg μl^{-1} RNA probe, plus 500 ng of either purified luciferase, Mettl3, Mettl14, or Mettl3 + Mettl14 in a 50 μl reaction and was incubated at 30 °C for 1 h. RNA was extracted using acid phenol and precipitated by ethanol. One-fifth of the precipitated RNA was used to measure c.p.m. in a scintillation counter.

Thin-layer chromatography. Thin-layer chromatography was used to confirm that the radioactivity detected was from m^{6}A and was performed as described previously[23] with modifications. Briefly, after the *in vitro* methylation assay, 3 μl of each RNA probe was digested into mononucleosides with nuclease P1, mixed with AMP and N^6-methyl-AMP standards (Sigma-Aldrich), loaded onto a PEI-Cellulose thin-layer chromatography plate (Millipore), and developed in isopropanol/HCl/water (70:15:15, v/v/v). After development, AMP and N^6-methyl-AMP spots were visualized under a UV-254 lamp (UVP; Supplementary Fig. 1D) and excised for measuring tritium activity using a scintillation counter.

Western analysis. Proteins were separated on SDS–PAGE gel, blotted onto PVDF membrane and detected with primary antibodies against Gapdh (Cell Signaling, catalogue number 5174, 1:20,000), Mettl3 (Bethyl Laboratories, catalogue number A301-567A, 1:5,000), Mettl14 (Sigma-Aldrich, catalogue number HPA038002, 1:5,000), flag (Sigma-Aldrich, catalogue number 1804, 1:10,000), His6 (Thermo, catalogue number MA1-21315, 1:5,000), HA (Roche Applied Science, catalogue number 11867423001 1:5,000) and HuR (Millipore, catalogue number 03-102, 1:5,000).

Co-immunoprecipitation of endogenous Mettl3 and Mettl14. Co-immunoprecipitation was conducted using a Pierce Crosslink IP kit (Thermo Scientific). Antibodies against Mettl3 (Bethyl Laboratories, catalogue number A301-567A), Mettl14 (Sigma-Aldrich, catalogue number HPA038002) or rabbit normal IgG (Millipore, catalogue number PP64B) were crosslinked to protein A/G agarose beads and then incubated with ∼2 mg of mESC lysates overnight at 4 °C. After washing and elution, input and IP products were analysed by western blots.

Reverse transcription coupled with quantitative PCR. DNase I-treated total RNA was used to synthesize cDNA using an iScript cDNA synthesis kit (Bio-Rad) according to the manufacturer's protocols. Quantitative PCR (qPCR) was performed with primer sets corresponding to the primer list table (Supplementary Table 3) and using iTaq Universal SYBR Green Supermix (Bio-Rad) on a BioRad CFX96 Touch Real-Time PCR Detection system.

RNA immunoprecipitation. RNA immunoprecipitation (RIP) was performed as described previously[22,24]. Antibodies used included 5 μg each of anti-HuR (Millipore, catalogue number 03-102), anti-Ago2 (Wako, catalogue number 01422023) or normal rabbit IgG (Millipore, catalogue number PP64B). qPCRs were carried out with the primer pairs listed in Supplementary Table 3.

Analysis of ESC self-renewal. mESCs (50,000 per well) were seeded in 6-well plates, and on days 2, 3, 4 and 5 cells were collected and counted. Alkaline phosphatase staining was performed with the Vector Red substrate kit (Vector Laboratories).

Fluorescence-activated cell sorting. Fluorescence-activated cell sorting analyses were performed as described previously[25]. Briefly, single-cell suspensions were obtained by repetitive pipetting and transfer through a 40 μm cell strainer. For AP activity analysis, cells were fixed in 4% paraformaldehyde for 2 min, washed twice with TBST and stained with the Vector Red substrate kit (Vector Laboratories) following the manufacturer's protocol and 1×10^4 cells were then analysed on a FACSAria cell sorter (BD Biosciences). Data were analysed with FACSDiva software (BD Biosciences). The cell population with a high AP activity signal—specifically the right half peak in the scramble sample—was gated as AP high and the percentage was calculated. For SSEA-1 analysis, cells were incubated with Alexa Fluor 488 anti-mouse SSEA-1 (BioLegend, catalogue number 125609) and 1×10^4 cells were analysed on a FACSAria.

Gene set enrichment analysis. Gene set enrichment analysis[26] was used to examine whether genes whose expression either increased or decreased following Mettl protein KD in mESCs were significantly enriched for the Oct4-centred PPI network or bivalent gene sets. These two gene sets and the microarray probe intensities in both KD cells and scramble controls were provided as input to the gene set enrichment analysis software (v2.0; http://www.broadinstitute.org/gsea) using default settings except that $\log_2$ fold-changes (rather than Signal2Noise) were used as metrics to rank the genes.

RNA stability assay. Actinomycin D (Sigma-Aldrich) at 5 μg ml^{-1} was added to mESCs 24 h after they were seeded in a 6-cm dish. After 0, 4 or 8 h of incubation, cells were collected and RNAs were isolated for qPCR or microarray analysis using an Affymetrix Genechip Mouse Gene 2.0 ST array.

RNA electrophoretic mobility shift assay. RNA electrophoretic mobility shift assay (EMSA) analysis was performed as described previously[22,24]. Briefly, 1 μg HEK293 purified HuR protein was incubated with end-labelled RNA probes for 30 min at room temperature, followed by separation of the mix on a 4% non-denaturing PAGE gel and exposure to a phosphor screen.

KD by siRNA transfection. J1 ESCs were seeded at 2×10^5 per well in 6-well plates and transfected with siRNAs using Lipofectamine RNAiMAX (Invitrogen) following the manufacturer's protocol. After 48 h, cells were reseeded and transfected again with siRNA. After another 48 h, cells were collected for analysis. siRNA target sequences for Mettl3, Mettl14 and HuR are listed below.

m^{6}A meRIP-seq. Total RNA was extracted using Trizol reagent (Invitrogen). RNA was treated with RNAse-free DNAse I (Roche) to deplete DNA contamination. PolyA RNA was purified using a GenElute mRNA Miniprep Kit (Sigma-Aldrich) as per the manufacturer's instructions. PolyA RNA was fragmented using a RNA fragmentation kit (Ambion). Two micrograms of fragmented RNA was saved as input. Two hundred micrograms of fragmented RNA was incubated with 3 μg anti-m^{6}A antibody (Synaptic Systems, catalogue number 202 003) in RIP buffer (150 mM NaCl, 10 mM Tris and 0.1% NP40) for 2 h at 4 °C, followed by the addition of washed protein A/G magnetic beads (Millipore) and incubation at 4 °C for a further 2 h. Beads were washed 6 times in RIP buffer and incubated with 50 μl immunoprecipitation buffer containing 0.5 mg ml^{-1} m^{6}AMP (Sigma-Aldrich)

DOI: 10.1038/ncb2902

to elute RNA. Immunoprecipitated RNA was extracted with phenol/chloroform and blinded samples were sent to the Next Gen Sequencing Core at Scripps Institute for library construction and high-throughput sequencing.

The Scriptseq v.2 RNA-seq Library Preparation method was performed on 40 ng of RNA for each sample. We followed the protocol given in the Scriptseq v.2 RNA-seq Library Preparation manual (Epicentre, an Illumina company), except DNA Clean & Concentrator-5 - PCR/DNA clean columns (Zymo Research) were used to isolate the cDNA before the PCR step. Fifteen cycles of PCR were performed on the cDNA and the resulting DNA products were purified on 2% E-Gel EX Agarose Gels (Invitrogen). The products were visualized using a blue-light transluminator and selected regions of the gel were excised corresponding to 200–400 bp products. The gel slices were dissolved in agarose-dissolving buffer and the DNA was isolated on DNA Clean & Concentrator-5 - PCR/DNA clean columns. The isolated DNA products were then analysed and quantified on an Agilent Bioanalyzer 2100. Samples were pooled and loaded into one lane of a HiSeq2000 v3 flowcell (Illumina) and sequenced for 100 bases with 7 separate index sequences to enable sequencing of 7 different samples on a single flow cell. The Genome Analyser Pipeline Software (Casava v1.8.2) was used to perform the preliminary data analysis of a sequencing run, which involves image analysis and base calling.

Quality control of raw read library. To improve the subsequent alignment quality, we devised an automated filtering program consisting of the following preprocessing steps. Reads containing non-determinant nucleotides (N) were filtered out using the fastx clipper from the FASTX-Toolkit (http://hannonlab.cshl.edu/fastx_toolkit/index.html). Bases lower than a defined Phred quality threshold (default: 20) at the 3′ end were trimmed off from each read using cutadapt (http://code.google.com/p/cutadapt/)[27]. Next, known Illumina primers and adaptor sequences were clipped off from each read by cutadapt, which computes sensitive semi-global alignments of all the reads against all the primer/adaptor sequences, allowing gapped and mismatched alignments. Finally, filtered reads were aligned against a custom contaminant list using Bowtie (0.12.7) to further filter contaminant reads mapped to mitochondrial, ribosomal, actin RNA or phi X genomes[28].

Alignment of filtered m^{6}A-seq read library to reference genome. Alignment to the mouse genome build mm10 was performed using TopHat (v2.0.6; ref. 29) with the following options:—max-multihits 1 (obtain uniquely mapped reads);—b2-very-sensitive (maximize alignment sensitive);—GTF provided with RefSeq gene annotation downloaded from UCSC Genome Browser for mm10 (13 May 2012) to improve detection of splicing junctions. To account for PCR artefacts, only reads aligned to the distinct genome coordinates were retained. This post-alignment filtering was achieved using samtools rmdup from Samtools (0.1.18; ref. 30) and MarkDuplicates from Picard (1.74) (www.picard.sourceforge.net/command-line-overview.shtml). As a result, the final processed alignments in each library comprise distinct reads each mapped to a unique location in the mm10 reference genome.

Quantifying gene expression to compute library correlation. The filtered reads after the above QC were subjected to quantification of gene expression based on RefSeq annotation downloaded from the UCSC Genome Browser (13 May 2012). A custom R script was developed to unambiguously count the reads that fall into each gene and subsequently computes RPKM (reads per kilobase of exon per million mapped reads) for each gene. The script makes use of the function summarizeOverlaps from the existing R package GenomicRanges. A pairwise correlation matrix (data not shown) was generated using the resulting expression matrix with rows as all of the RefSeq genes and columns as the samples corresponding to immunoprecipitate and control replicates.

Visualization of peaks and plotting. Alignments were converted to bedGraph using genomeCoverageBed from BedTools[31] then to tdf (tiled data file) to visualize the peaks as per-base coverage across the genome using the Integrative Genome Viewer[32] (Fig. 2a). Unless mentioned otherwise, all of the plots were generated using the R package ggplot2.

Peak calling. To identify strand-specific reads-enriched regions or peaks in the m^{6}A-immunoprecipitate relative to the control or input library, we applied MACS to reads on '+' and '-' strands separately[33]. MACS was run with default options except for—nomodel,— shiftsize = 25, and—gsize 'mm' to turn off fragment size estimation (only applicable to double-stranded DNA), to make window size 25 bp (which was chosen empirically to obtain peaks of median size around 200 nt), and to base peak calling on mouse reference genome size, respectively. The strand-specific peaks from MACS were then pooled for each library. The pooled peaks from m^{6}A-IP libraries were subject to a stringent cutoff requiring each peak to have an FDR (estimated by MACS) <0.1. The fold-enrichment calculated from MACS for each filtered peak was scaled by the corresponding fold-change of the ActB gene in terms of RPKM to control for differential base-line expression between the immunoprecipitate libraries. We then compared peaks from scramble control (CTL) with peaks from KD. For the peaks overlapped between the two libraries, we calculated the relative fold-enrichment as the fold-change of the scaled fold-enrichment in KD relative to the scaled fold-enrichment in CTL. The Mettl3/14-associated peaks are peaks only in CTL (but not in KD) or having negative relative fold-enrichment. The latter indicates decreased peak intensity in KD relative to CTL (see Supplementary Table 1). Finally, peaks from replicate libraries were combined.

Mettl3/14 target genes in mESC. The Mettl3/14-associated peaks obtained above were used to overlap with known Ensembl genes using the R/Bioconductor packages biomaRt and GenomicRanges[34]. Unique Ensembl gene IDs corresponding to Mettl3- and Mettl14-associated peaks were identified as Mettl3 and Mettl14 target genes, respectively. We compared Mettl3/14 target genes to obtain genes targeted by both Mettl3 and 14 or exclusive to only one of the two enzymes (Fig. 2b). In addition, Mettl3/14 target genes were imported to the DAVID online server for GO enrichment analysis[35] (Fig. 2f).

Microarray analysis. DNA-free total RNA was extracted and blinded samples were sent to the Analytical Genomics core facility at the Sanford Burnham Medical Institute (Lake Nona) for microarray analysis. Raw data (in CEL files) from Affymetrix Genechip Mouse Gene 2.0 ST arrays were imported into the R environment and normalized by RMA function using the Bioconductor package *oligo*. Differential expression analysis between Mettl3/14 KD and scrambled control (CTL) at 0 h (h) was performed using limma[36]. A cutoff of adjusted P value by Benjamini–Hochberg or q-value <0.1 and $\log_2$ fold-change greater and less than 0 was used to determine respectively upregulated and downregulated genes with at least one of the probes having q-value <0.1. In addition, a heat map was drawn based on the significant probes with q-value <0.01 using the R package *gplots* (Fig. 3d). To compare relative RNA levels at time points 4 and 8 h in KD and CTL samples, we further normalized the expression values by ActB expression and by the corresponding expression at 0 h to control for differential base-line expression and initial abundances, respectively (Fig. 4b). Genes with increased stability (Figs 3e and 5a,h) due to Mettl3/14 KD were determined as those having higher normalized expression in KD versus CTL at 8 h.

Association between methylation and expression. Fisher's exact test was performed to test for a significant association between Mettl3/14 target genes identified by the meRIP-seq analysis (Peak calling) and upregulated genes (Microarray analysis). Specifically, Ensembl gene IDs were compared among both gene lists to obtain a 2-by-2 contingency table comprising the numbers of genes that are (not) methylated and (not) upregulated or downregulated at 0 h. The R built-in function fisher.test (x, alternative = 'greater') P.value was then used to obtain the $-\log_{10}(P \text{ value})$ (Fig. 4a).

Comparison with bivalent, Oct4-PPI genes, HuR and Ago2 target genes. We examined whether Mettl3/14 target genes are significantly enriched for bivalent genes and genes involved in the Oct4-centric PPI network as follows. RefSeq mRNA IDs for the bivalent genes in mESCs were obtained from Supplementary Table 2 in ref. 13. Common symbols for genes involved in the Oct4-centric protein–protein interaction (PPI) network were collected from Supplementary Tables 1, S6-9 in ref. 14. Assuming that the number of Mettl3/14 target genes identified in the mESCs that are also bivalent or in the Oct4-PPI network follows a hypergeometric distribution, we computed the significance of enrichment using the R built-in function phyper (…, lower.tail = FALSE; Fig. 4c). All of the RefSeq transcripts and Ensembl genes were used as the backgrounds for the bivalent and Oct4-PPI enrichment analysis, respectively. Different databases were used in the two analyses to be consistent with the IDs generated from the original studies. The same enrichment was tested for Mettl3/14 target genes with increased stability (Microarray analysis; Fig. 4e).

Similarly, we performed hypergeometric tests for enrichment of the Mettl3/14+HuR putative target genes among genes with increased stability based on the number of stabilized Mettl3/14 target genes with 3′UTR harbouring or depleted of the canonical HuR motif AUUUA located within the corresponding Mettl3/14-associated peaks[37] (Fig. 5a). Finally, Mettl3/14 targets with increased stability were tested for enrichment of Ago2 target genes overlapped by Ago2-CLIP-seq clusters in combined wild-type mESC libraries[21] (http://rowley.mit.edu/pubs/Ago2_CLIP/bed_files_3UTR/; Fig. 5h).

^{35}S-methionine metabolic labelling. ESCs were washed three times with DPBS (Gibco) and incubated for 30 min at 37 °C with DMEM without methionine and cystine (Gibco) and supplemented with 10% dialysed FBS (Gibco), followed by incubation with 10 uCi ml^{-1} EasyTag EXPRESS ^{35}S Protein Labelling Mix (Perkin Elmer) for 4 h at 37 °C. Cells were washed three times with DPBS and lysed in CelLytic buffer (Sigma-Aldrich). Lysate protein concentrations were determined by the Bradford method (Fermentas), and 15 μg of lysate proteins was separated on two 10% polyacrylamide gels. One was stained using Coomassie blue and the other one was exposed to a phosphor screen and scanned using a FujiFilm FLA-5100 imager.

Flag- and HA-tagged Mettl3 or Mettl14 co-immunoprecipitation. HEK293 cells transiently co-transfected with constructs encoding flag- and HA- tagged Mettl3 (or Mettl14) were collected 48 h after transfection. Immunoprecipitation from cell lysates was performed with anti-flag M2 magnetic beads (Sigma-Aldrich, catalogue number M8823) following the manufacturer's protocol. Input and immunoprecipitation products were analysed by western blot to determine whether flag- and HA-tagged Mettl3 or Mettl14 dimerize by themselves.

Protein purification from baculoviral-infected Sf9 insect cells. Baculoviruses expressing either His6–luciferase, His6–Mettl14 or Flag–Mettl3 were generated using the Bac-to-Bac Baculovirus Expression System (Invitrogen). Hi5 insect cells (Invitrogen; 10^6 cells ml^{-1}, 50 ml cultures) were co-infected with these viruses (His6–luciferase + flag–Mettl3 or His6–Mettl14 + Flag–Mettl3) at a high multiplicity of infection (>10) for 48 h. Cells were collected by centrifugation at 1,000*g* and resuspended in Ni-NTA wash buffer (50 mM HEPES, at pH 8.0, 300 mM NaCl, 10 mM imidazole and 1 mM dithiothreitol) containing 0.2% IGEPAL CA-630. After clarification by centrifugation and filtration, hexahistidine-tagged proteins were purified through Ni-NTA chromatography (Qiagen) with the use of Ni-NTA wash buffer containing 250 mM imidazole for elution. Fractions containing His6–luciferase or His6–Mettl14 + Flag–Mettl3 were desalted into 25 mM HEPES, at pH 7.6, 100 mM NaCl, 1 mM $MgCl_2$, 1 mM dithiothreitol and 10% glycerol using a HiTrap Desalting Column (GE Healthcare).

shRNA RNA sequences. Mettl3: 5′-CGTCAGTATCTTGGGCAAATT-3′; Mettl3 no. 2: 5′-GGAGATCCTAGAGCTATTAAA-3′; Mettl3 no.3: 5′-GCACACTG-ATGAATCTTTAGG-3′; Mettl14: 5′-GCATTGGTGCTGTGTTAAATA-3′; Mettl14 no.2: 5′-CCTGAGATTGGCAATATAGAA-3′; Mettl4: 5′-TTTCCGATCTGAGC-TATTTAA-3′; HuR no.1: 5′-CATTGGGAGAACGAATTTAAT-3′; HuR no.2: 5′-CGAGGTTGAATCTGCAAAGCT-3′; HuR no.3: 5′-GCCAATCCCAACCAGAA-CAAA-3′.

siRNA sequences. Mettl3: 5′-GGACTGCGATGTGATTGTA-3′, 5′-GACGAATT-ATCAATAAGCA-3′; Mettl14: 5′-CCGGATGTACAGAGGAAAT-3′, 5′-GGGAACT-CATCAGACTAAA-3′, 5′-GCACCTCGGTCATTTATAT-3′; HuR siRNA: 5′-CAGTTTCAATGGTCATAAA-3′, 5′-ATGTGAAAGTGATTCGTGA-3′, 5′-GCTT-ATTCGGGATAAAGTA-3′; Scramble: 5′-TTCTCCGAACGTGTCACGT-3′.

Data access. Data have been deposited in NCBI's Gene Expression Omnibus (GEO) and are accessible through GEO series accession number GSE46880.

22. Zhao, J., Sun, B. K., Erwin, J. A., Song, J. J. & Lee, J. T. Polycomb proteins targeted by a short repeat RNA to the mouse X chromosome. *Science* **322,** 750–756 (2008).
23. Harper, J. E., Miceli, S. M., Roberts, R. J. & Manley, J. L. Sequence specificity of the human mRNA N6-adenosine methylase *in vitro*. *Nucleic Acids Res.* **18,** 5735–5741 (1990).
24. Zhao, J. *et al.* Genome-wide identification of polycomb-associated RNAs by RIP-seq. *Mol. Cell* **40,** 939–953 (2010).
25. Wang, Y. *et al.* Reprogramming of mouse and human somatic cells by high-performance engineered factors. *EMBO Rep.* **12,** 373–378 (2011).
26. Subramanian, A. *et al.* Gene set enrichment analysis: a knowledge-based approach for interpreting genome-wide expression profiles. *Proc. Natl Acad. Sci. USA* **102,** 15545–15550 (2005).
27. Martin, M. Cutadapt removes adapter sequences from high-throughput sequencing reads. *EMBnet J.* **17,** 10–12 (2011).
28. Langmead, B., Trapnell, C., Pop, M. & Salzberg, S. L. Ultrafast and memory-efficient alignment of short DNA sequences to the human genome. *Genome Biol.* **10,** R25 (2009).
29. Trapnell, C., Pachter, L. & Salzberg, S. L. TopHat: discovering splice junctions with RNA-Seq. *Bioinformatics* **25,** 1105–1111 (2009).
30. Li, H. The Sequence Alignment/Map format and SAMtools. *Bioinformatics* **25,** 2078–2079 (2009).
31. Quinlan, A. R. & Hall, I. M. BEDTools: a flexible suite of utilities for comparing genomic features. *Bioinformatics* **26,** 841–842 (2010).
32. Robinson, J. T. *et al.* Integrative genomics viewer. *Nature Publishing Group* **29,** 24–26 (2011).
33. Zhang, Y. *et al.* Model-based analysis of ChIP-Seq (MACS). *Gen. Biol.* **9,** R137 (2008).
34. Durinck, S., Spellman, P. & Birney, E. Mapping identifiers for the integration of genomic datasets with the R/Bioconductor package biomaRt. *Nat. Protocol.* **4,** 1184–1191 (2009).
35. Huang, D. W., Sherman, B. T. & Lempicki, R. A. Systematic and integrative analysis of large gene lists using DAVID bioinformatics resources. *Nat. Protocol.* **4,** 44–57 (2009).
36. Smyth, G. in *Bioinformatics and Computational Biology Solutions Using R and Bioconductor* (eds Gentle- man, R., Carey, V., Dudoit, S., Irizarry, R. & Huber, W.) 397–420 (Springer, 2005).
37. Mukherjee, N. *et al.* Integrative regulatory mapping indicates that the RNA-binding protein HuR couples pre-mRNA processing and mRNA stability. *Mol. Cell* **43,** 327–339 (2011).

DOI: 10.1038/ncb2902

nature cell biology

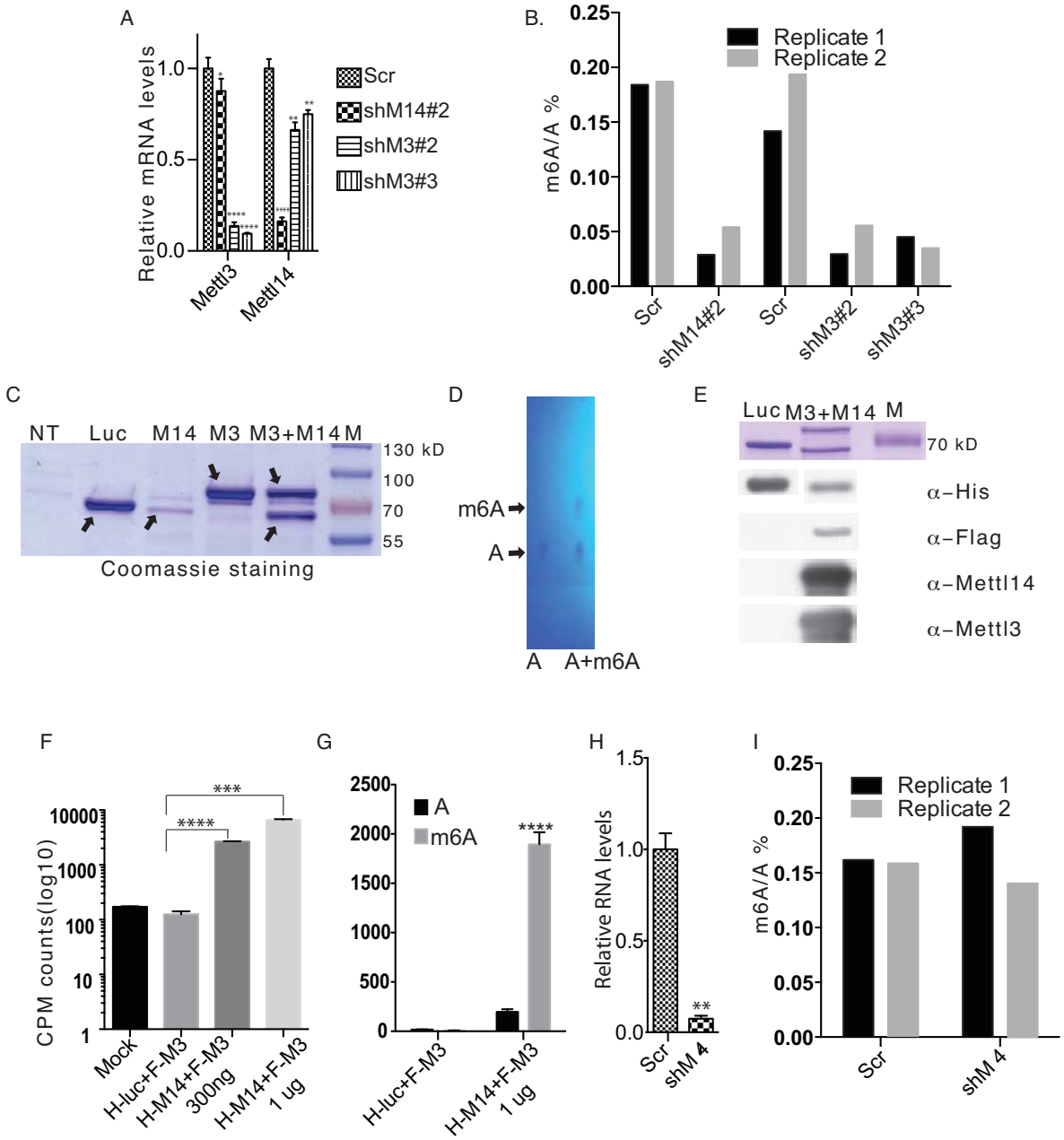

Supplementary Figure1 Supplements for Figure 1. **A.** RT-qPCR analysis of mESCs expressing shRNAs targeting Mettl3 or Mettl14. Scr: scramble. shM14#2: shRNA against Mettl14; shM3#2 and shM3#3, shRNAs against Mettl3. **B.** Measurement of percentage m^6A/A ratio in kd and control cells based on LC-MS/MS. **C.** Coomassie staining of proteins purified from whole cell lysates of HEK293 cells overexpressing luciferase (Luc), Mettl3 (M3), Mettl14 (M14), and Mettl3 plus Mettl14. NT: no transfection control. M: Marker. Arrows show protein of the expected size. The original gel is shown in Supplementary Fig.5. **D.** Visualization of the separated A versus m^6A standards by TLC. **E.** Panels from top to bottom: First panel, Commassie staining showing his-tagged proteins purified from Sf9 cell lysates co-expressing his-tagged luciferase + flag-tagged Mettl3 or his-tagged Mettl14 + flag-tagged Mettl3. Remaining panels: flag, his, Mettl3, and Mettl14 western blots of the same proteins shown in Coomassie staining. Luc, luciferase; M3, Mettl3; M14, Mettl14. The original gel is shown in Supplementary Fig.5. **F.** CPM counts of RNA probes extracted after the *in vitro* methylation assay. **G.** TLC analysis showing CPM counts of excised m^6A spots from digested RNA probes used in the methylation assay. **H.** RT-qPCR analysis of cells expressing a shRNA targeting Mettl4 versus scramble control. **I.** Measurement of a percentage representing m^6A/A ratio in Mettl4 kd and control cells using mass spectrometry. Scr: scramble. shM4: shRNA targeting Mettl4. Error bars from panels A and F-H represent means ± SEM from 3 separate experiments. One-tailed Student's *t*-test, $^{**}P < 0.01$, $^{***}P<0.001$, $^{****}P < 0.0001$ vs. scramble control. Scr: scramble.

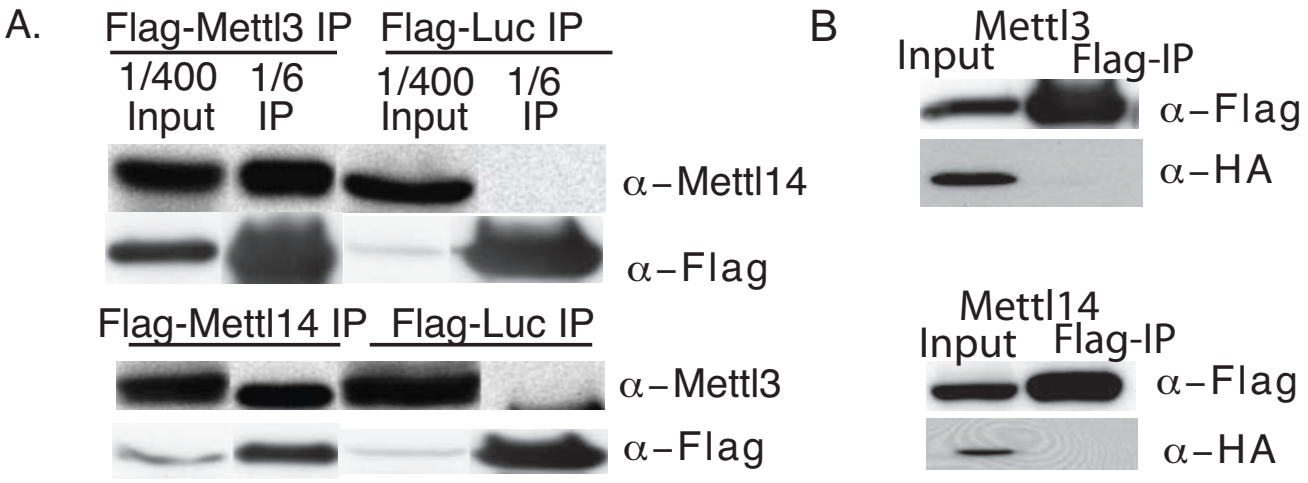

Supplementary Figure2 Supplement for Figure 2. **A.** Mettl3 or Mettl14 western immunoblots of IP'ed samples using M2 beads and lysates of HEK293 cells overexpressing flag-tagged Mettl3, Mettl14, or luciferase. Luc, luciferase. The original gel is shown in Supplementary Fig.5. **B.** Flag or HA western blots of co-IP'd samples using M2 beads and lysates of HEK293 cells overexpressing either flag- and HA-tagged Mettl3 or flag- and HA- Mettl14. The original gel is shown in Supplementary Fig.5.

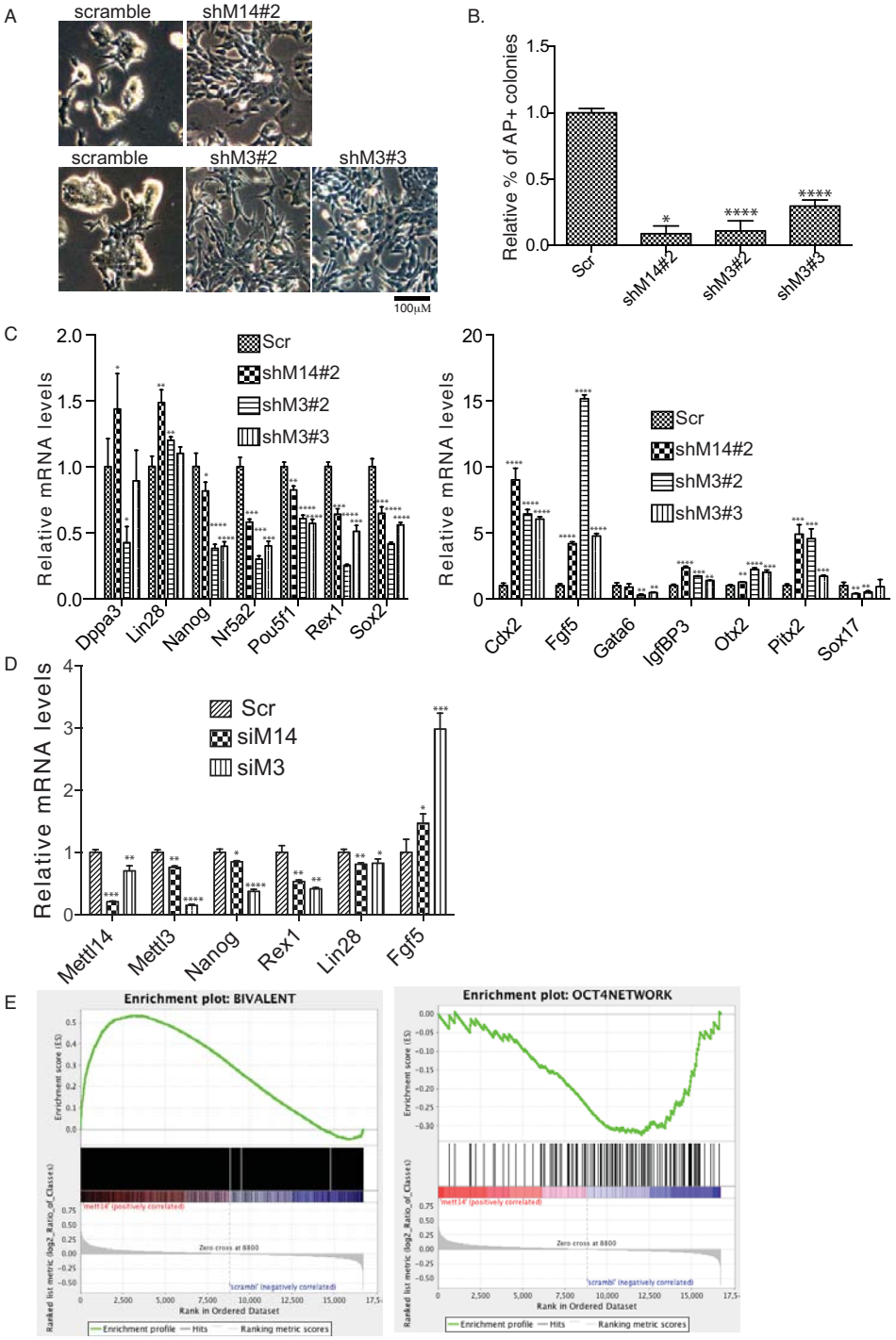

Supplementary Figure3 Supplement for Figure3. **A.** Phase contrast microscopy showing mESC colony morphology in indicated kd versus control cells. Scale bars, 100 μm. shM14#2, additional shRNA targeting Mettl14; shM3#2-3 additional shRNAs targeting Mettl3. **B.** Quantification of AP-positive colonies. Scr, Scramble. **C.** RT-qPCR analysis of pluripotency (left) and differentiation (right) genes in kd versus control cells. **D.** RT-qPCR analysis showing decreased expression of Mettl3, Mettl14, and the pluripotency genes Nanog, Rex1, and Lin28, and increased expression of the differentiation gene Fgf5 in siRNA transiently-transfected kd versus control cells. Scr: scramble; siM3: siRNAs against Mettl3; siM14: siRNAs against Mettl14. **E.** GSEA analysis showing enrichment of gene sets of developmental regulators (left) and pluripotency-related genes (right) in Mettl14 kd versus control cells. A False Discovery Rate (FDR) <0.162 was calculated for bivalent genes and of FDR<0 for pluripotency-related genes. Note that a FDR<0.25 is statistically significant for GSEA analysis: www.broadinstitute.org/gsea/doc/GSEAUserGuideFrame.html. Scale bars, 100 μm. Error bars from panels B-D represent mean ± SEM from 3 separate experiments. One-tailed Student's *t*-test, $*P < 0.05$, $**P < 0.01$, $***P < 0.001$, $****P < 0.0001$ vs. scramble control. Scr: scramble.

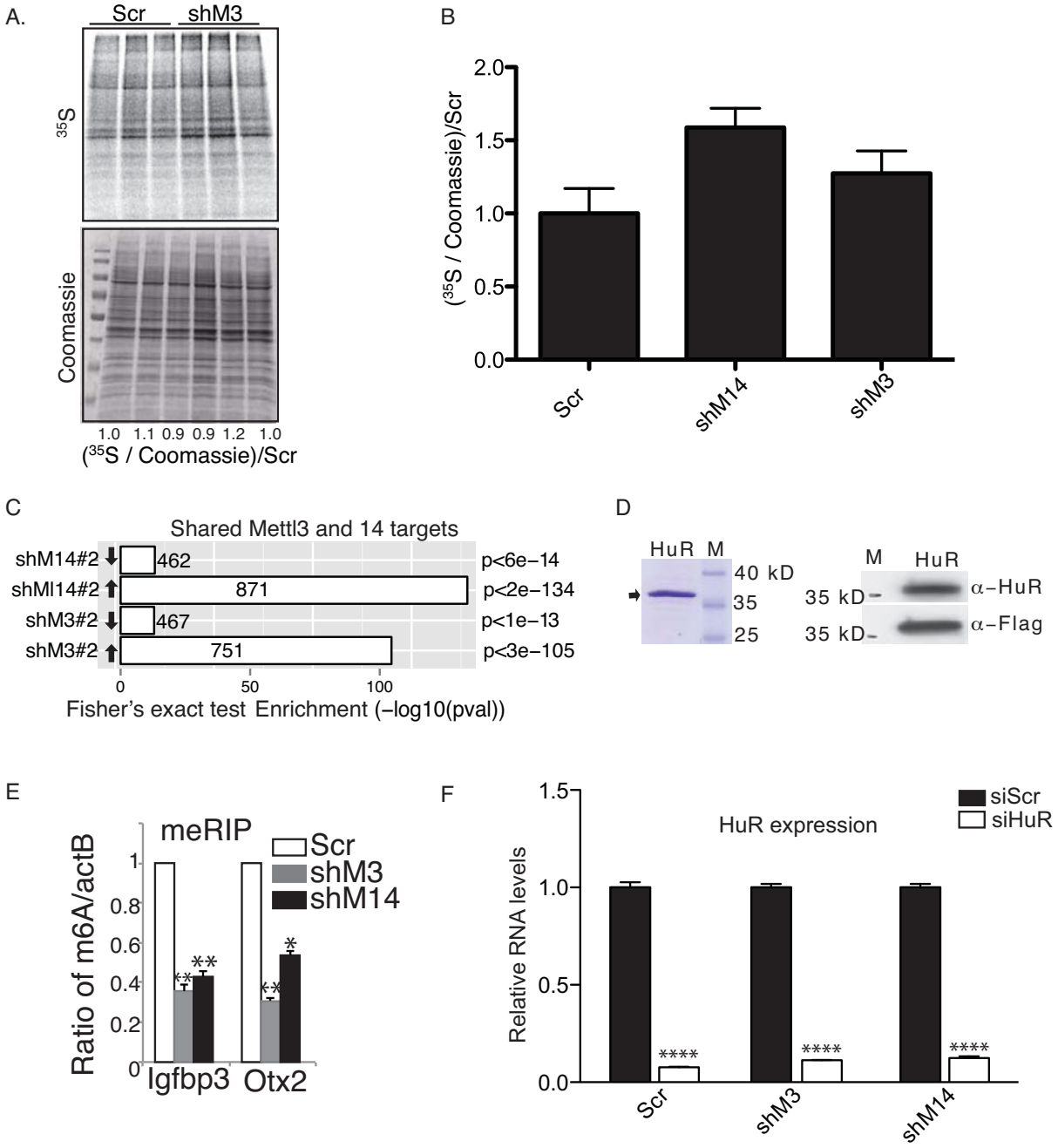

Supplementary Figure4 Supplements for Figures 4 and 5. **A.** Representative SDS-PAGE gel showing the amount of ^{35}S incorporated into newly synthesized proteins in Mettl3 kd versus control cells after ^{35}S-pulse-labeling for 4 hrs. Upper panel: intensity of ^{35}S radioactivity after exposure SDS-PAGE gel to phosphoimager. Lower panel: Coomassie staining as a loading control. Numbers at the bottom show the ratio of incorporated radioactivity (upper panel) to corresponding Coomassie staining (lower panel) after normalized to scramble control. Band intensity was quantified using the Image J program. **B.** Summary of quantification of ^{35}S labeling in kd and control cells. Scr, Scramble. shM3, shRNA targeting Mettl3; shM14, shRNA targeting Mettl14. **C.** Enrichment of up- or down-regulated Mettl3 and Mettl14 targets in kd versus control cells. Arrows indicate up- or down regulation of gene expression. shM14#2, second shRNA against Mettl14; shM3#2, second shRNA against Mettl3. **D.** Coomassie staining (left) and western blots of (right) HuR protein purified from whole cell lysates of HEK293 cells overexpressing flag-tagged HuR. M: Marker. The original gel is shown in Supplementary Fig.5. **E.** meRIP-qPCR showing methylation status of Igfbp3 and Otx2 in both Mettl3 and Mettl14 kd versus control cells. **F.** RT-qPCR analysis of HuR expression following HuR knockdown with siRNA in Mettl3 kd, Mettl14 kd, and control knockdown cells. Scr: scramble. Erro bars from panels E-F represent means ± SEM from 3 separate experiments. One-tailed Student's *t*-test, $*P < 0.05$, $**P < 0.01$, $***P < 0.001$, $****P < 0.0001$ vs. scramble control. Scr: scramble.

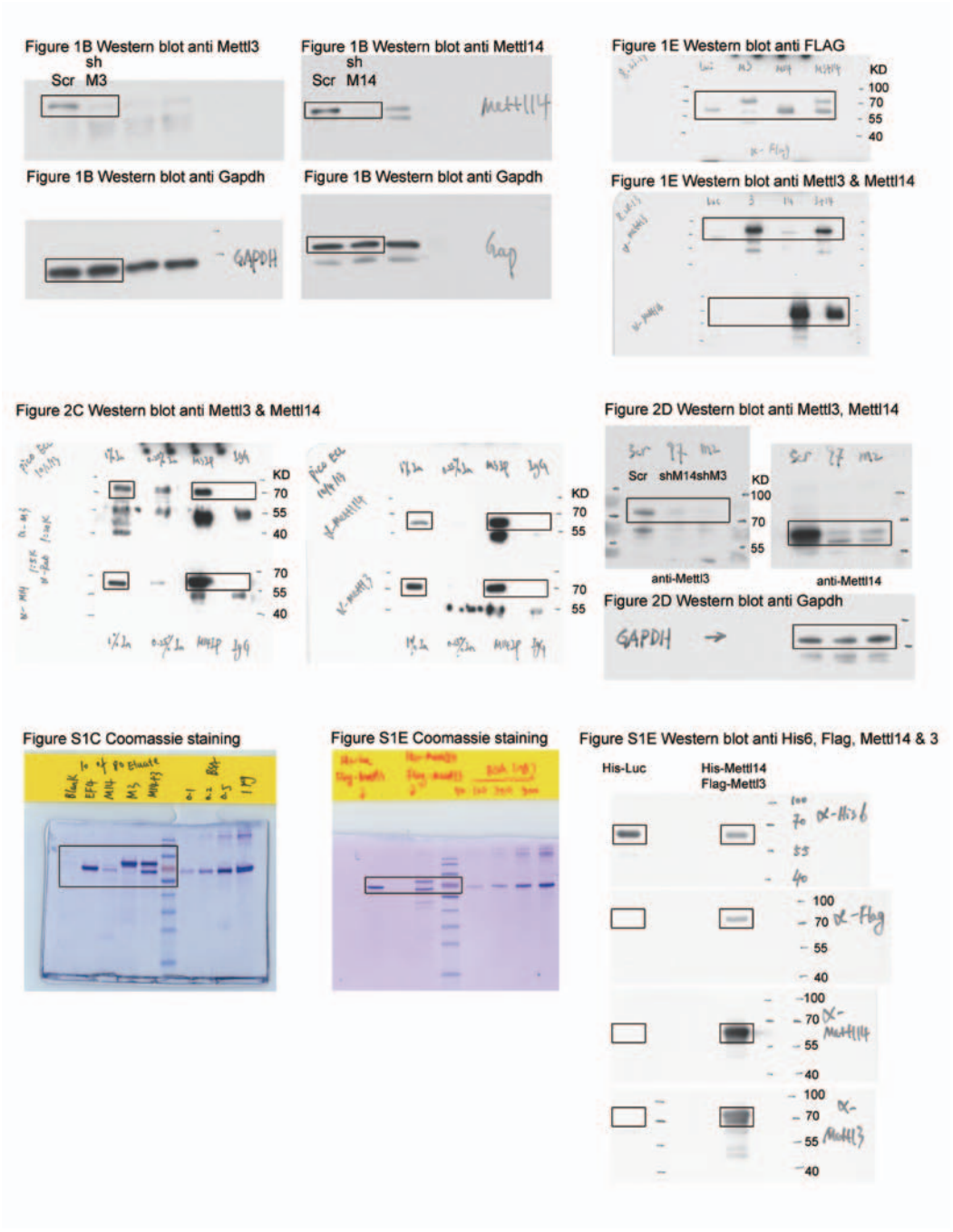

Supplementary Figure5 Uncropped western blots and Coomassie stainings.

Figure S2A Western blot anti FLAG, Mettl3 & Mettl14

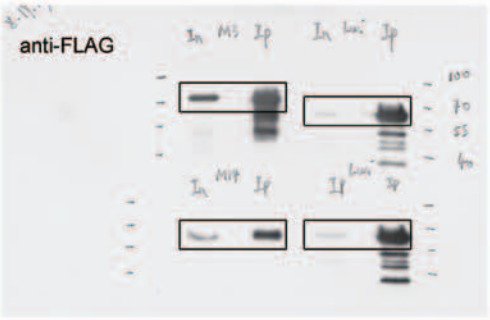

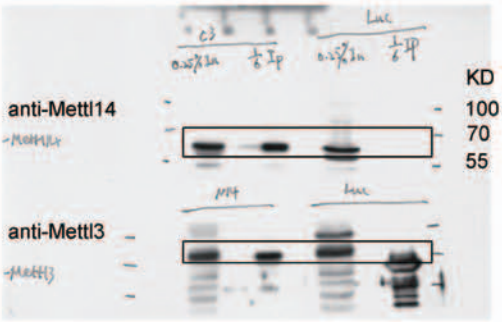

Figure S2B Western blot anti Flag

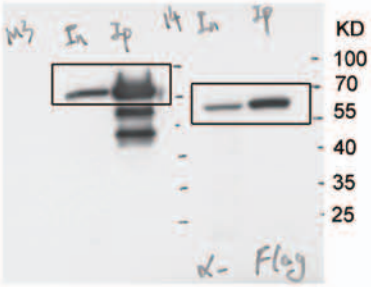

Figure S2B Western blot anti HA

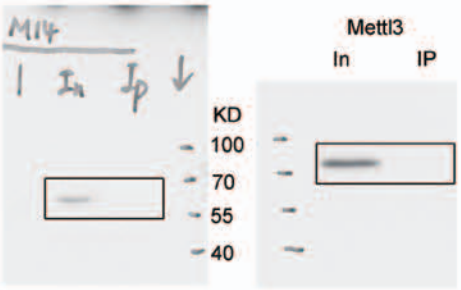

Figure S4D Coomassie staining

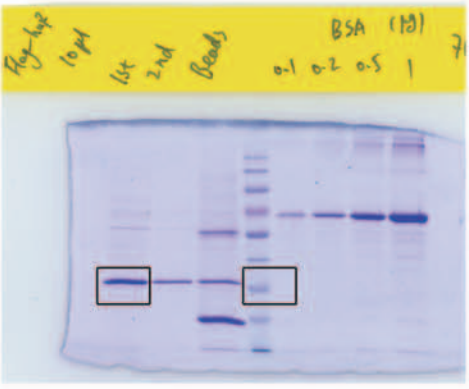

Figure S4D Western blot anti huR & FLAG

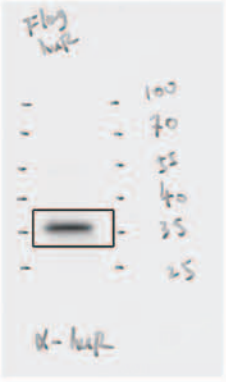

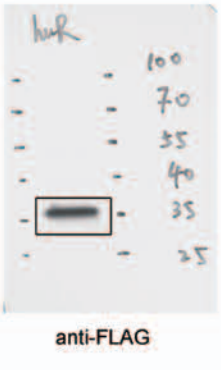

Supplementary Table Legends

Supplementary Table1 Genes showing decreased number and/or intensity of methylation peaks in Mettl3 kd and Mettl14 kd versus scramble control. Chromosomal coordinates (column 1-4) indicate the peak locations in the scramble control library. All peaks pass the FDR < 0.1 cutoff from MACS. When two peaks from the control and Mettl3 or Mettl14 kd overlap, we calculated the relative fold-enrichment (RFE) in kd relative to control (Methods), and listed only the peaks showing a decreased RFE in kd (i.e., RFE < 0). For peaks only present in control, RFE is #N/A. For known genes overlapped by the peaks, ensembl gene id and common gene names are shown.

Supplementary Table2 Microarray analysis of Mettl3 kd and Mettl14 kd versus scramble control cells treated with Actinomycin D for 4 and 8 hrs relative to 0 hr.

Supplementary Table3 List of qPCR primers used in this study.